



Representative elementary surface for morphology and permeability of natural rock fractures

Wei Li¹ · Zhechao Wang¹ · Liping Qiao¹ · Jinjin Yang¹ · Jiajia Li¹

Received: 19 December 2021 / Accepted: 21 March 2023 / Published online: 5 April 2023
© Springer-Verlag GmbH Germany, part of Springer Nature 2023

Abstract

Fracture surface morphology, mechanical and hydraulic properties are related to fracture size. One of the core issues in the size effect is the representative elementary surface, which determines the size of the test specimens in the laboratory and facilitates the application of test results to the field. In this study, the size effect on surface morphology and permeability of rock fractures is investigated, and the representative elementary surface size for the surface morphology and the permeability was determined based on the asperity height data of fracture surfaces obtained by 3D laser scanning in the field. The roughness of fracture surfaces varies significantly at small fracture surface sizes. As the fracture surface size continues to increase, the fracture surface roughness tended toward a relatively stable state. The critical size for fracture surface roughness stability in the study, which is called the representative elementary surface, is 300–400 mm. The size effect on the permeability of rock fractures was investigated, and the results show that fracture permeability tended toward a relatively stable state with increasing fracture size, which was the same as the fracture surface roughness. The representative elementary surface size for fracture permeability is less than 100 mm in the study, which is also less than that for fracture surface roughness with the same coefficient of variation. This result indicated that a lower coefficient of variation might provide the best estimate of the representative elementary surface for fracture permeability compared with the fracture surface roughness.

Keywords Surface roughness · Rock fracture · Permeability · Size effect · Representative elementary surface · Coefficient of variation

Introduction

The sizes of natural fractures range from micrometers to several hundred kilometers (Berkowitz 2002; Lei et al. 2015), and the surface morphology, mechanical and hydraulic properties of fractures exhibit a strong correlation with the size of fractures (Dou et al. 2019; Feng et al. 2022; Giwelli et al. 2009; Liu et al. 2017; Tsang and Witherspoon 1983; Wei et al. 2021; Yang et al. 2001; Zou et al. 2015). One of the core issues in the size effect of geometric and physical properties of fracture surface is the representative elementary surface (RES), beyond which the geometric and physical properties of the fracture surface reach a relatively stable

state (Esmaili et al. 2010; Wang et al. 2018a, b). Accurately obtaining the RES size will help in determining the size of test specimens in the laboratory and facilitate the application of test results to the field to solve oil/gas production and storage (Chen et al. 2019; Singh and Cai 2018; Wang et al. 2018a), geothermal energy extraction (Pandey et al. 2018), grouting activities (Wu et al. 2019; Zou et al. 2020) and other problems.

The strength, deformation and permeability properties of rock fractures depend on the fracture surface morphology (Giwelli et al. 2009; Lin et al. 2019; Luo et al. 2016; Vogler et al. 2018). There are many quantitative characterizations of fracture surface morphology, including the joint roughness coefficient (JRC) curve (Alameda-Hernández et al. 2014; Barton 1973; Tatone and Grasselli 2010; Zhang et al. 2014), statistical parameters of asperity height (Kulatilake et al. 2006; Thomas 1981; Wang et al. 2020; Zhao et al. 2018) and fractal parameter (Babanouri et al. 2013; Brown and Scholz 1985; Liu et al. 2020; Odling 1994). The size effect on fracture surface morphology was investigated by

✉ Zhechao Wang
wang_zhechao@hotmail.com;
wangzhechao@mail.neu.edu.cn

¹ Key Laboratory of Ministry of Education on Safe Mining of Deep Metal Mines, Northeastern University, 11#, 3rd Ave, Wenhua Rd, Shenyang, Liaoning 110004, China

many experts and scholars (Li et al. 2020b; Özvan et al. 2014; Yang et al. 2001). Nigon et al. (2017) analyzed the multiscale characterization of fracture surface roughness and found that the standard deviation of asperity height and characteristic length of fracture surfaces decreased with size. Chen et al. (2015a) used the sill value and variable range of a variogram to describe the fracture surface roughness JRCv and obtained JRCv for different sizes of fracture surfaces. Their results showed that JRCv decreased with fracture surface size. Yan et al. (2020) proposed a new parameter AHD (the average equivalent height difference) to characterize the fracture surface roughness, and the relation between AHD and fracture surface size was the same as that between JRCv and size proposed by Chen et al. (2015a). The above research on the size effect of fracture surface roughness and hydraulic behavior shows that the fracture surface morphology changes with the fracture size. However, as the fracture size continues to increase, the fracture surface morphology tends toward a relatively stable state, as has been found by some experts and scholars. Fardin et al. (2001) analyzed the size effect on fracture surface roughness by the relation between fractal dimension D and fracture surface size. The parameter D first decreased and then tended to be constant with the fracture surface size. Chen et al. (2015a) found that the JRCv value remained constant when the size was larger than a threshold value. However, the threshold value, i.e. the RES size for fracture surface roughness or morphology, was not given, and the method of determining the RES size is not clear.

The mechanical and hydraulic behaviors of fractures also exhibit a strong correlation with the size (Dou et al. 2019; Liu et al. 2017; Tsang and Witherspoon 1983; Zou et al. 2015). Raven and Gale (1985) conducted tests on fluid flow in a natural fracture under normal loading conditions. The flow rate decreased with the fracture size and the deviation from cubic increased with the fracture size. Qian et al. (2007) studied the hydraulic conductivity of a single fracture with different fracture sizes, surface roughness, apertures and hydraulic gradients. Their results showed that the

hydraulic conductivity increased linearly with the fracture size. Giwelli et al. (2009) investigated the effect of fracture size on closure behavior under normal stresses of 10 MPa. Their results showed that the standard deviation of the aperture increased with the fracture size and did not reach a constant value. Huang et al. (2018) simulated the fluid flow in fractures with different sizes, and the simulation results showed that the permeability changed significantly first and then tends to become stable with increasing the size of the fracture model. These studies indicate that the fracture surface roughness and hydraulic behavior remain constant when the fracture size exceeds a critical size. The above studies show that a RES for the mechanical or hydraulic behaviors of fractures exists. However, the relations between RES for fracture surface morphology and mechanical or hydraulic behaviors are not clear.

The size effect on the surface morphology and permeabilities of rock natural fractures was investigated in this study. The 3D laser scanning process performed on fracture surfaces in the field and the method of data processing are introduced. Then, the size effect on the natural fracture surface morphology was analyzed. The size effect on fracture surface morphology was emphasized, and the RES for fracture surface morphology was obtained. Finally, the numerical simulation of fluid flow in fractures was carried out based on the fracture model established by scanned fracture surface data. The size effect on the permeability was analyzed, and the results were compared with the size effect on the fracture surface roughness.

Data acquisition

3D laser scanning of a natural fracture surface

The scanned natural fracture surfaces were selected from Gongchangling District, Liaoyang City, Liaoning Province, China. The scanned fracture surfaces are located in three areas, numbered A, B and C, as shown in Fig. 1. The

Fig. 1 Natural fracture surface selected for this study



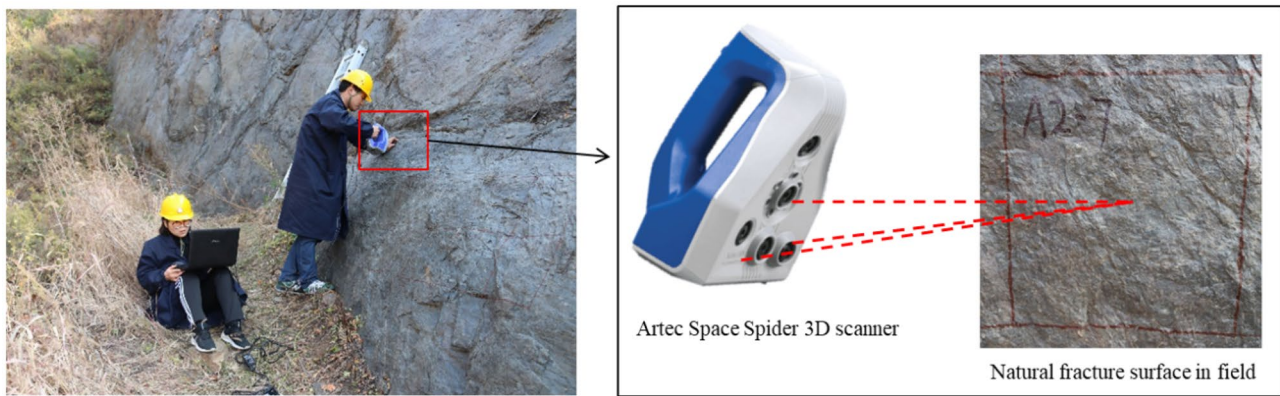


Fig. 2 Scene and method of laser scanning in the field

lithology of the three areas is quartz sandstone. The scanned fracture surface is located on the surface and is a secondary fracture surface formed by weathering. The rock weathering in area A is more serious than that in the other two areas. To be noted, B and C are adjacent, and A is tens of kilometers from the other two areas.

The scene and method of laser scanning in the field are shown in Fig. 2. The three-dimensional topography of the selected fracture surface was scanned by an Artec Space Spider 3D scanner. The scanned fracture surface is zoned in the field to better scan with required size, and the number of fracture surface in Fig. 2 is A2–7. Limited by the field conditions and computer memory, the size of the scanned fracture surface was approximately 300 × 300 mm. The 3D point cloud images of fracture surfaces were obtained after calibration and denoising. Then the topography point cloud image of the fracture surface was reconstructed by the interpolation function in MATLAB. These processes are shown in Fig. 3. In Fig. 3, from left to right, there are photo of natural fracture surface, scan results, cloud image after calibration and denoising, and reconstructed cloud image in MATLAB.

A total of 104 fracture surfaces with a size of 300 × 300 mm was scanned, including 43 fracture surfaces in area A, 12 fracture surfaces in area B and 49 fracture surfaces in area C. The number of point clouds on each fracture surface after calibration and denoising was approximately 150000–220000, and the mean sampling interval was estimated to be approximately 0.64–0.77 mm. Because of the complexity of the fracture surfaces and the application of multi-view scanning automatic splicing technology, the point cloud of the splicing positions is denser than that of other positions. The sampling intervals of the 3D point cloud images of the fracture surface after calibration and denoising are not uniform, which is not conducive to subsequent research. It is necessary to use an interpolation function to reconstruct the topography point cloud image of the fracture surface in MATLAB to obtain equidistant point cloud data. The optimal sampling interval in MATLAB is determined as follows.

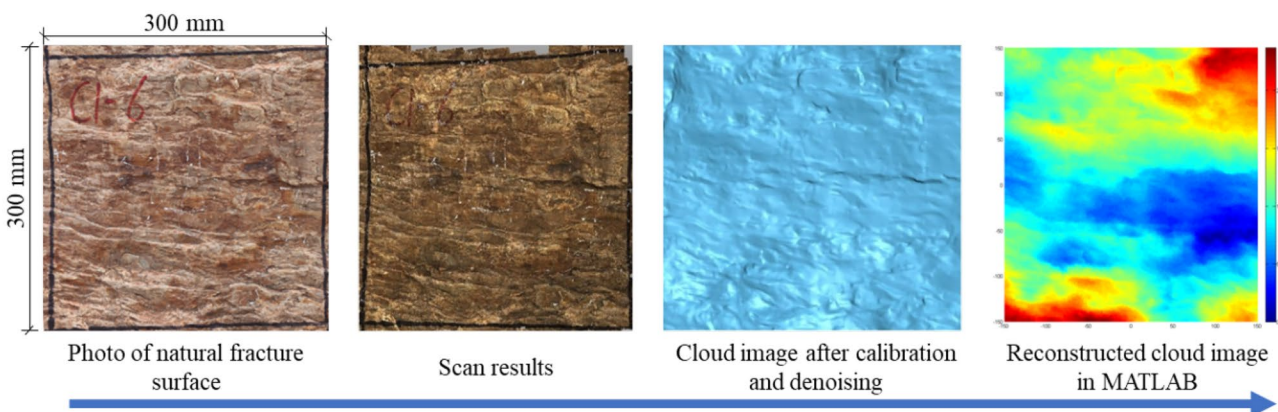


Fig. 3 Data acquisition process of fracture surface

Determination of the sampling interval of the fracture surface

The root mean square of the first derivative of the asperity Z_2 is used to characterize the roughness of the two-dimensional fracture surface, which is expressed as follows (Li et al. 2020a; Li and Zhang 2015; Liu et al. 2016; Wang et al. 2016):

$$Z_2 = \frac{1}{(n-1)(\Delta x)^2} \sqrt{\sum_{i=1}^n (z_{i+1} - z_i)^2} \tag{1}$$

where, z_i is the asperity height at point i , n is the number of point clouds, Δx is the distance in the axial direction between points $i + 1$ and i . The distance is the sampling interval, and it is constant in this study. The scanned fracture surfaces are in the 3D domain; thus, Z_2 can be extended to 3D form as Z_{2s} , which is expressed as (Belem et al. 2000; Zhao et al. 2020):

$$Z_{2s} = \left\{ \frac{1}{(n_x-1)(n_y-1)} \left[\frac{1}{\Delta x^2} \sum_{i=1}^{n_x-1} \sum_{j=1}^{n_y-1} \frac{(z_{i+1,j+1} - z_{i,j+1})^2 + (z_{i+1,j} - z_{i,j})^2}{2} + \frac{1}{\Delta y^2} \sum_{i=1}^{n_x-1} \sum_{j=1}^{n_y-1} \frac{(z_{i+1,j+1} - z_{i+1,j})^2 + (z_{i,j+1} - z_{i,j})^2}{2} \right] \right\}^{1/2} \tag{2}$$

where, n_x and n_y are the number of point clouds along the x -axis and y -axis, respectively. Δy is the sampling interval along the y -axis, which is equal to Δx in this study. Z_{2s} is used to characterize the fracture surface when determining the sampling interval. To facilitate comparison with the results of permeability characteristics, Z_2 is used to characterize the fracture surface roughness when the size effect and anisotropy of roughness are investigated.

Ten fracture surfaces were randomly selected among the 104 scanned fracture surfaces, whose numbers are A1-6, A2-8, A3-4, A5-9, B7-2, B7-10, C1-7, C3-1, C5-3 and C6-6. The three-dimensional roughness Z_{2s} of the ten fracture surfaces were obtained with different sampling intervals and were shown in Fig. 4. The roughness Z_{2s} decreases with the sampling interval. When the sampling interval is more than 0.9 mm, the fracture surface roughness Z_{2s} tends to become stable (Rong et al. 2013; Sutopo et al. 2002). The attenuation rate mentioned in Song et al. (2017) was used to determine the optimal sampling interval. The attenuation rate of the fracture surface roughness was calculated according to Eq. (3).

$$\Delta SP = \frac{|SP_i - SP_c|}{SP_c} \times 100\% \tag{3}$$

where, ΔSP is the attenuation rate of a statistical parameter, and the parameter in the study is the fracture surface roughness. SP_i is the statistical parameter value of the i th sampling interval. SP_c is the statistical parameter value at

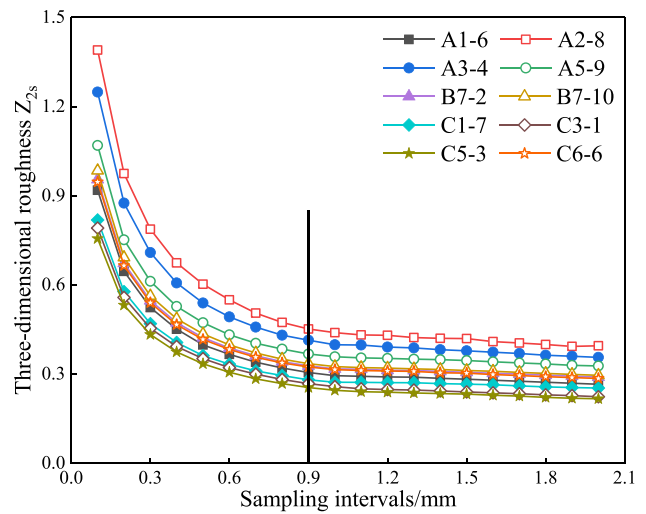


Fig. 4 Relation between sampling intervals and three-dimensional roughness Z_{2s} of 10 randomly selected fracture surfaces

critical sampling intervals, which is the value at the minimum sampling interval generally. Based on the mean sampling interval of field scanning, i.e. 0.64–0.77 mm, the critical sampling intervals need larger than the mean sampling interval and were determined as 0.8 mm in the study. The attenuation rate of fracture surface roughness was obtained, as shown in Fig. 5.

The relation between sampling intervals and roughness attenuation rate of 10 randomly selected fracture surfaces is shown in Fig. 5. The attenuation rate increases with sampling intervals. When the sampling interval is between 0.8 and 1.0 mm, the attenuation rate is less than 10%, which is a

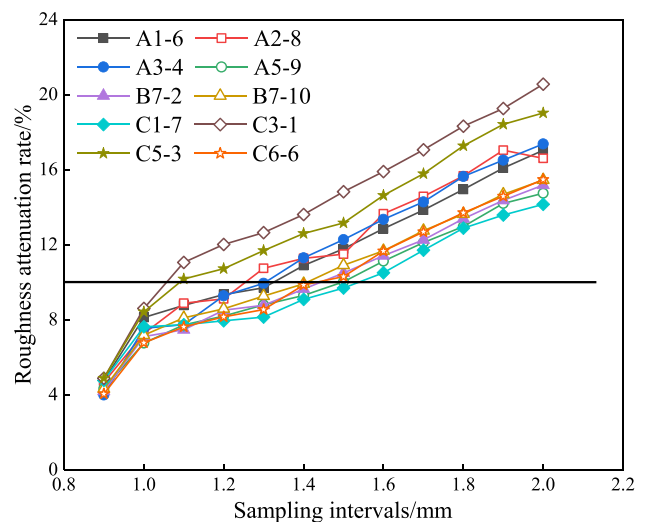


Fig. 5 Relation between sampling intervals and roughness attenuation rate of 10 randomly selected fracture surface

reasonable sampling interval (Song et al. 2017). Considering the above results and calculation efficiency, the optimal sampling interval is 1 mm in the study.

Large-scale fracture surface morphology data

The adjacent fracture surfaces were selected and spliced into two fracture surfaces with the size of 900 × 900 mm, which are numbered A2 and C3, respectively. Reconstructed topography point cloud images of the two fracture surfaces were shown in Fig. 6.

Characterization of fracture surface morphology

Distribution of asperity height

The parameters of fracture surface morphology include the asperity height (Chen et al. 2015b; Song et al. 2020), roughness Z_2 and Z_{2s} . The spatial and statistical distributions of asperity height of three fracture surfaces are shown in Fig. 7. The results of height distribution parameters and roughness of fracture surface are shown in Table 1.

Figure 7 shows that the spatial distribution of asperity height is uneven, and the statistical results show that they follow the normal distribution. The range of asperity height is -24.67 to 28.45 mm on fracture surface A2 and -14.96 to 12.42 mm on fracture surface C3. The asperity standard deviation of the two fracture surfaces is 3.953 and 2.742 mm, respectively. The height standard deviation of the C3 fracture surface is smaller than that of A2. The roughness Z_{2s} of fracture surface A2 and C3 are 0.386 and 0.237, respectively. The fracture surface A2 is rougher than fracture surface C3 due to more serious rock weathering. The order of two fracture surface roughness is consistent with the height standard

deviation. It indicates that the fracture surface roughness is positively correlated with height standard deviation.

Anisotropy of fracture surface roughness

The topography of the natural rock fracture surface is complex, and the roughness along different directions is different, i.e. the roughness of fracture surfaces has directionality. The roughness Z_2 in different directions (Chen et al. 2016; Song et al. 2017) was calculated according to Eq. (1), as shown in Fig. 8. The direction interval is 10°, and the roughness of each fracture surface was calculated in 36 directions.

Figure 8 shows that the roughness in different directions on the same fracture surface is different. A dimensionless parameter, discontinuity anisotropic coefficient (DAC), is selected to quantitatively describe the anisotropy of fracture surface roughness. it is expressed as (Song et al. 2017):

$$DAC = 1 - \frac{1}{e^{CV_{Z_2}}} \tag{4}$$

where, CV_{Z_2} is the variation coefficient (Baghbanan and Jing 2007; Fakhimi and Gharahbagh 2011) of roughness Z_2 in 36 directions. The range of DAC values is [0, 1). When $DAC=0$, the roughness of the fracture surface is isotropic. When $0 < DAC < 1$, the roughness of the fracture surface is anisotropic. The larger the DAC value is, the more anisotropic the fracture surface is. The DAC values of three fracture surfaces were obtained according to Eq. (4) and are shown in Table 1. The DAC values of the two fracture surfaces are 0.042 and 0.027, respectively. The degree of anisotropy is ranked as follows: $C3 < A2$, which is the same as the height standard deviation. It indicates that the anisotropy of a fracture surface is positively correlated with its height standard deviation.

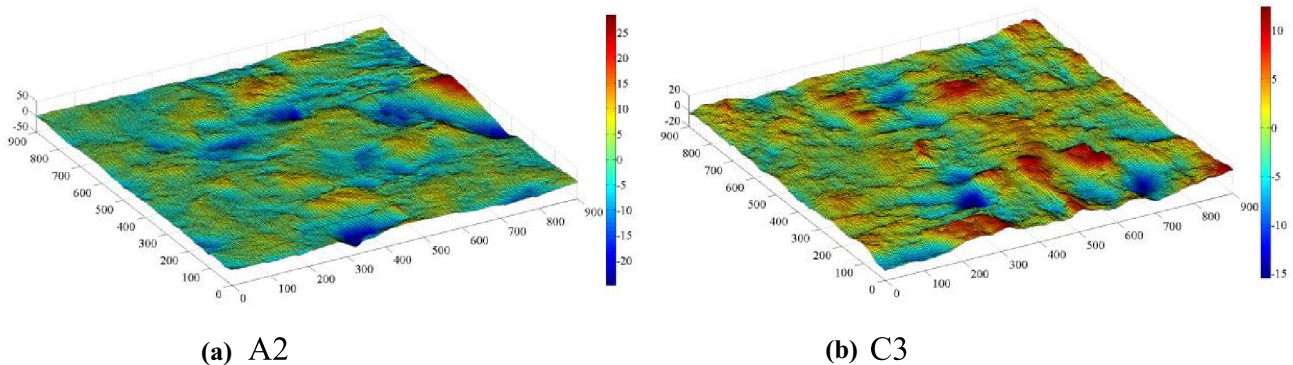
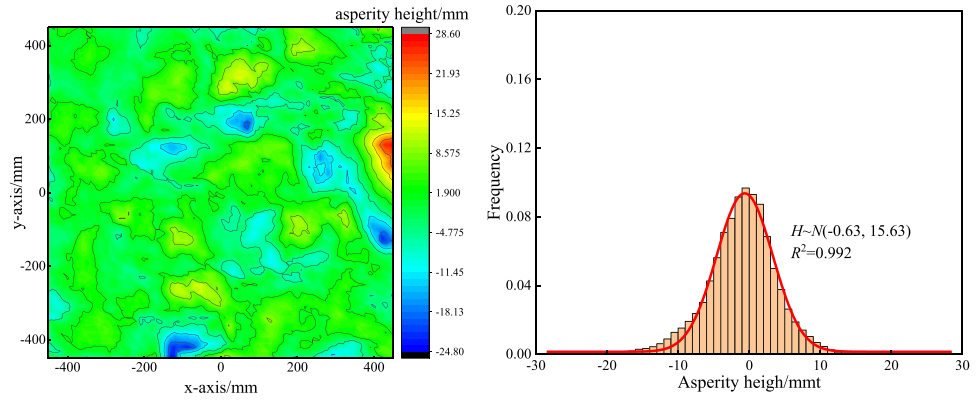
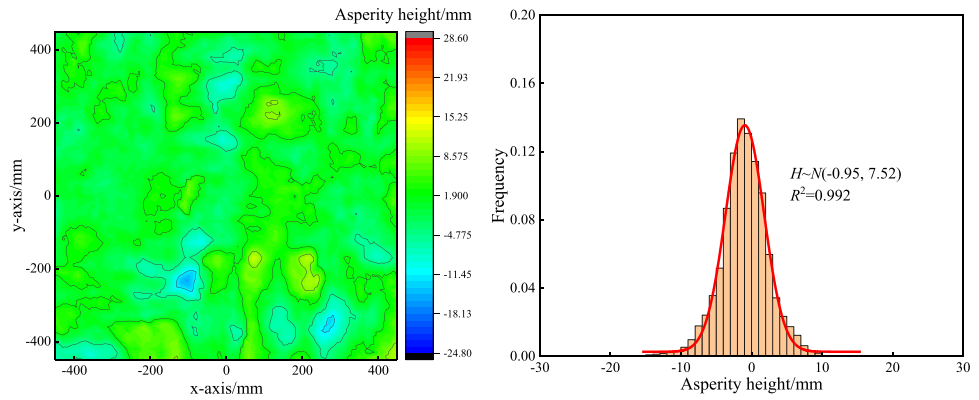


Fig. 6 Reconstructed topography point cloud image of the fracture surface (a) A2 and (b) C3 (Unit: mm)

Fig. 7 Spatial and statistical distribution of asperity height on (a) A2 and (b) C3 fracture surface



(a) A2



(b) C3

Size effect on fracture surface roughness

Size effect on the asperity height distribution

To obtain the distributions of asperity height with different fracture surface sizes, the “base” fracture surface was discretized into sampling fracture surfaces of various sizes in rectangular coordinate systems, as shown in Fig. 9 (Baghbanan and Jing 2007; Wang et al. 2018a, b). The “base” and sampling fracture surface are all squares. The size of the fracture surface is represented by the side length for convenience in the following study. The size of

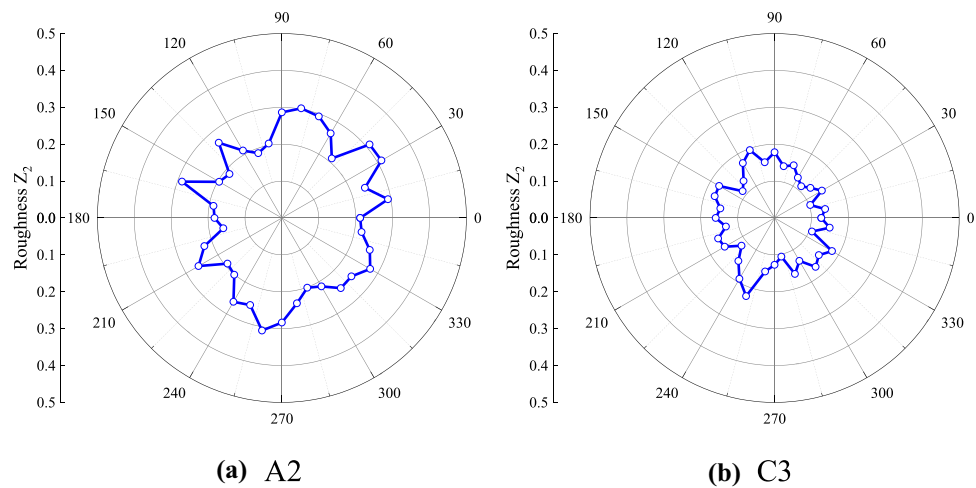
the “base” fracture surface is 900 mm, and the sizes of the sampling fracture surfaces range from 100 to 800 mm with an interval of 100 mm. Ten sampling fracture surfaces of each size are obtained at different positions to eliminate the contingency. The statistical asperity height distributions for each sampling fracture surface were obtained, as shown in Fig. 10. Figure 10 shows the results of fracture surface C3.

When the size of the fracture surface is small, the distributions of asperity height do not completely follow a normal distribution. With the increase of fracture surface size, the distribution law tends to be consistent. When the size of the fracture surface $L \leq 300$ mm, the distributions of asperity height in different positions and with different fracture surface sizes are different. When $300 \text{ mm} < L < 600$ mm, the distributions of asperity height in different positions with the same fracture surface sizes are consistent, but with different fracture surface sizes, they are different. When the size of the fracture surface $L \geq 600$ mm, the distributions of asperity height in different positions and with different fracture surface sizes are different. The asperity height fitting parameters with different sampling fracture surfaces were obtained to investigate a method for determining the above

Table 1 Statistics of fracture surface parameters

| No | Asperity height | | Roughness Z_{2s} | Anisotropic parameter | |
|----|-----------------|-----------------------|--------------------|------------------------------------|---|
| | Mean/mm | Standard deviation/mm | | Coefficient of variation CV_{Z2} | Discontinuity anisotropic coefficient DAC |
| A2 | -0.634 | 3.953 | 0.386 | 0.043 | 0.042 |
| C3 | -0.953 | 2.742 | 0.237 | 0.028 | 0.027 |

Fig. 8 Roughness Z_2 of fracture surface (a) A2 and (b) C3 in different directions



critical sizes, i.e. 300 and 600 mm. The relation between the standard deviation of asperity height and fracture surface sizes is shown in Fig. 11. In Fig. 11, the S1–S10 represent 10 different positions, the marks with different shapes represent the standard deviation results at different positions, the solid line represents the mean value of the standard deviation at the 10 positions and the dotted line represents the variation coefficient of that. The standard deviation of asperity height varies significantly at small fracture surface sizes. As the fracture surface size increases, the variation in the standard deviation gradually decreases to approximately 2.74 mm, which is the standard deviation of the asperity height of “base” fracture surface.

When the fracture surface size $L \leq 300$ mm, the variation coefficient of the standard deviation $CV_\sigma > 15\%$. When the fracture surface size $L \geq 600$ mm, the variation coefficient of the standard deviation $CV_\sigma < 5\%$. The critical sizes can be determined by the coefficient of variation (CV). In general, the variability of a parameter is weak, and a relatively stable state occurs when $CV \leq 15\%$ (Baghbanan and Jing 2007; Koyama and Jing 2007; Liang et al. 2019). When the size

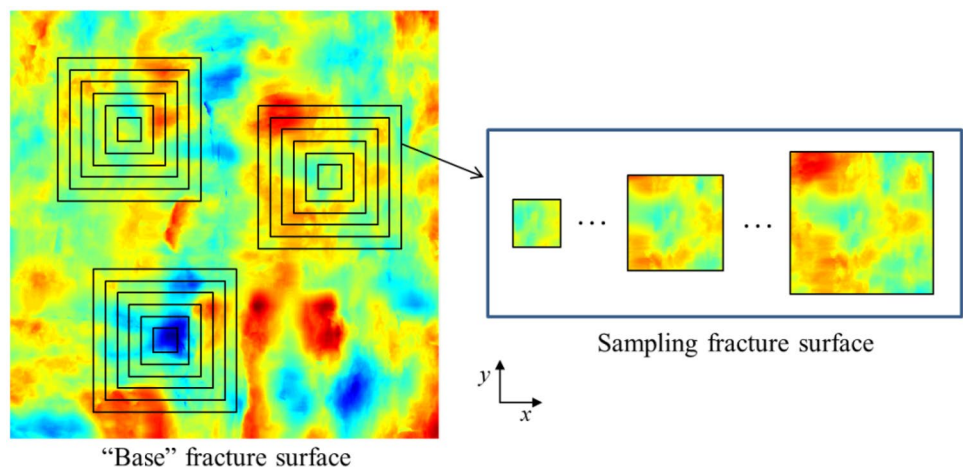
of the fracture surface is larger than 400 mm, the asperity height distribution parameters of the fracture surface are in a relatively stable state. The critical size is 400 mm for stable asperity height distribution, i.e. the RES size for the asperity height distribution is approximately 400 mm (Esmaili et al. 2010; Wang et al. 2018a, b). If the sampling interval is smaller than 100 mm, a more accurate RES size will be obtained. For fracture surface A2, the results are similar to those for fracture surface C3, as shown in Table 2.

Table 2 Sizes of the fracture surfaces with different variation coefficients of standard deviation for fracture surfaces A2 and C3.

Size effect on fracture surface roughness

To analyze the size effect on fracture surface roughness, the sampling fracture surface roughness along the x-axis and y-axis were calculated. The acquisition method of the sampling fracture surface is shown in Fig. 9. Z_2 is calculated according to a fracture profile on the fracture surface. The mean value \bar{Z}_2 of all fracture profiles along a certain

Fig. 9 Method of obtaining the sampling fracture surface with different sizes from the “base” fracture surface



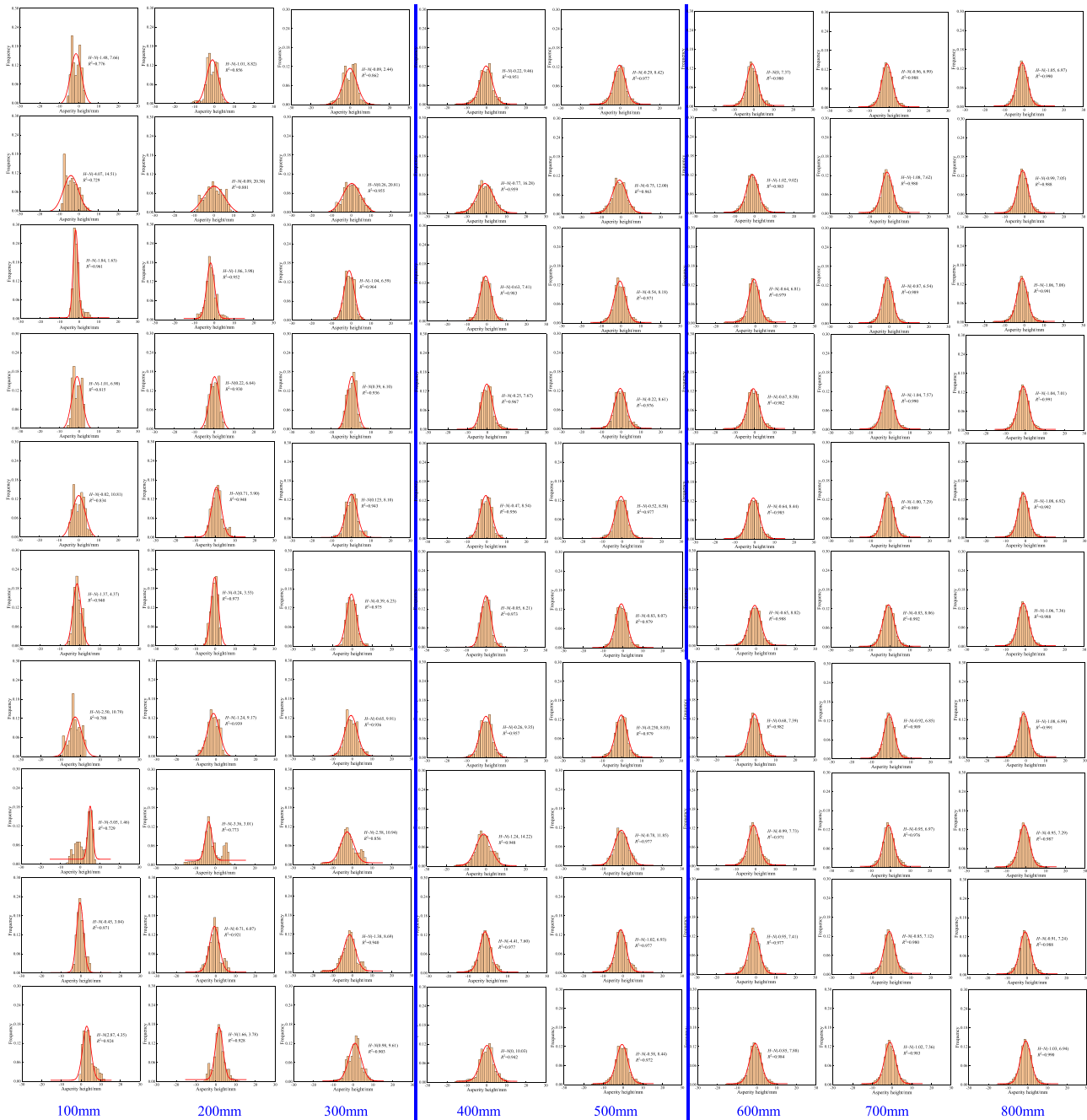


Fig. 10 Statistical distributions of asperity height with different fracture surface sizes on fracture surface C3

direction of the fracture surface is the roughness in that direction, as shown in Fig. 12. The calculation equation of roughness is shown in Eq. (5).

$$\bar{Z}_2 = \sum_{i=1}^n Z_{2,i} \tag{5}$$

where, $Z_{2,i}$ is the root mean square of the first derivative of asperity height in the i th fracture profile.

The roughness of the sampling fracture surfaces along the x-axis and y-axis were obtained, as shown in Fig. 13. The ranges of roughness on fracture surfaces A2 and C3 with different sizes is 0.126–0.307 and 0.137–0.353 along the x-axis and 0.091–0.324 and 0.082–0.234 along the y-axis, respectively. The roughness of fracture surfaces varies significantly at small fracture surface sizes. As the fracture surface size continues to increase, fracture surface roughness tends to move to a relatively stable state. The roughness variation coefficient

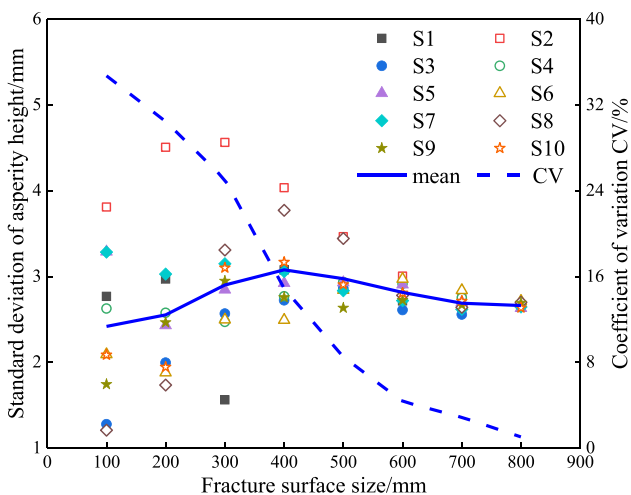


Fig. 11 Relation between the standard deviation of asperity height and fracture surface sizes

of 15% and difference between the sampling size and the next sampling size of 5% are taken as the criterion for the roughness to enter a stable state (Baghbanan and Jing 2007; Koyama and Jing 2007; Liang et al. 2019). The RES sizes of roughness are 300, 400, 300 and 300 mm, respectively. The roughness RES size of fracture surface A2 is slightly larger than that of fracture surface C3. The equivalent fracture surface roughnesses, which are the fracture surface roughnesses under the stable state, are 0.243, 0.267, 0.178 and 0.153, respectively.

Size effect on the anisotropy of the fracture surface roughness

The roughness Z_2 of sampling fracture surfaces in different directions was obtained to analyze the size effect on the anisotropy of the fracture surface roughness. The DAC of the sampling fracture surfaces was obtained, as shown in Fig. 14. The solid and dotted line represent mean value and variation coefficient of DAC in Fig. 14. The DAC varies with the fracture surface sizes. The variation coefficient of DAC first decreased and then increased slowly with the fracture surface size. When the fracture surface size L is larger than 300 mm, the variation coefficient of DAC is less than 30% and even less than 15% in some fracture surface sizes,

Table 2 The sizes of fracture surface under different variation coefficient of standard deviation for fracture surface A2 and C3

| Variation coefficient of standard deviation CV_σ | Fracture surface size L /mm | |
|---|-------------------------------|-----------------|
| | C3 | A2 |
| $CV_\sigma > 15\%$ | $L \leq 300$ | $L \leq 300$ |
| $5\% < CV_\sigma \leq 15\%$ | $300 < L < 600$ | $300 < L < 600$ |
| $CV_\sigma \leq 5\%$ | $L \geq 600$ | $L \geq 600$ |

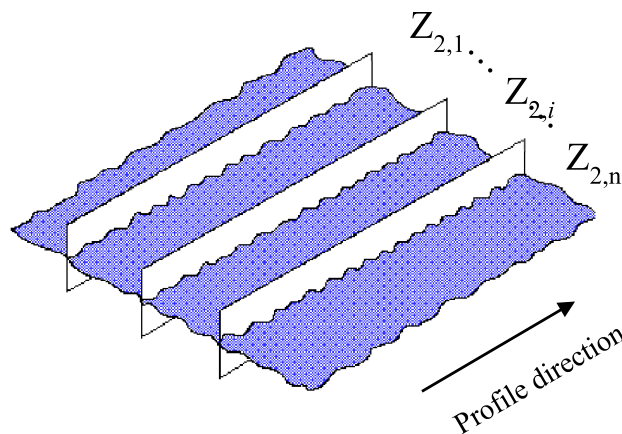


Fig. 12 Calculation method of fracture surface roughness in a certain direction

which indicates that the RES size for the anisotropy of the fracture surface roughness may be 300–400 mm.

Size effect on fracture permeability

Governing equation

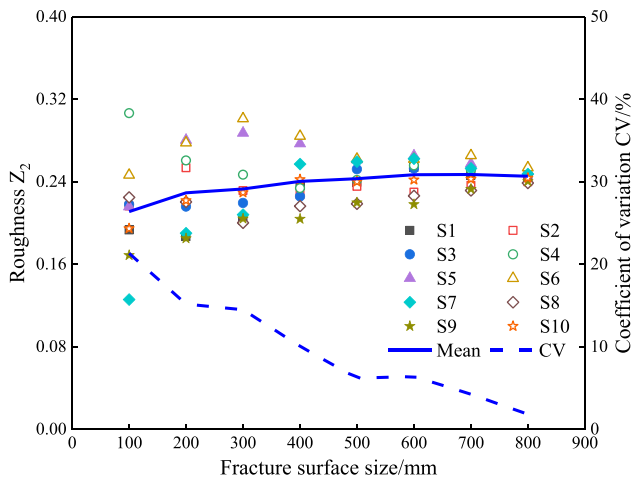
The fluid flow in fractures is generally governed by nonlinear Navier–Stokes equations. However, it is difficult to solve fluid flow in natural rough fractures with complex geometry. For the fluid flow in a fracture with a pair of smooth parallel surfaces, the Navier–Stokes equations can be simplified to the cubic law, which is expressed as (Huang et al. 2018; Liu et al. 2021; Witherspoon et al. 1980):

$$Q = -\frac{e^3}{12\mu} \nabla P \tag{6}$$

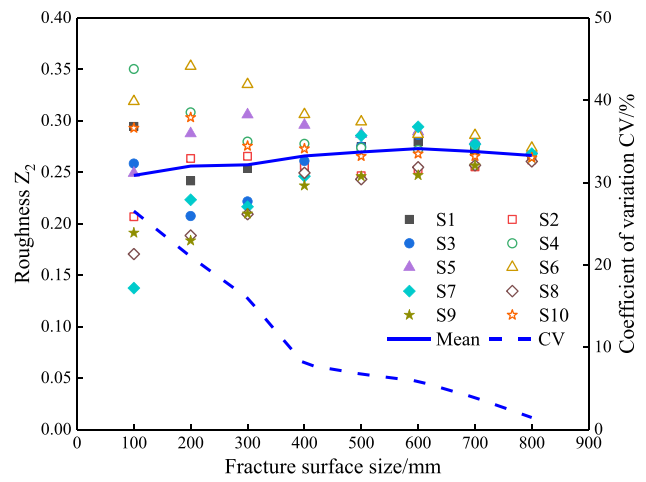
where Q is flow rate, e is hydraulic aperture, μ is dynamic viscosity coefficient, P is fluid pressure in fracture. A natural fracture consists of two rough fracture surfaces, where the cubic law is over-simplified. When flow velocity is low and the fracture surface does not vary too abruptly, the local cubic law, which is also called Reynolds equation, can be used to describe the flow in fractures. The Reynolds equation is shown in Eq. (7) (Brown 1987; Huang et al. 2017) and is used to analyze the fluid flow in rough fractures. The permeability k of a rough fracture can be calculated by Eq. (8) (Huang et al. 2018).

$$\nabla(e^3 \nabla P) = 0 \tag{7}$$

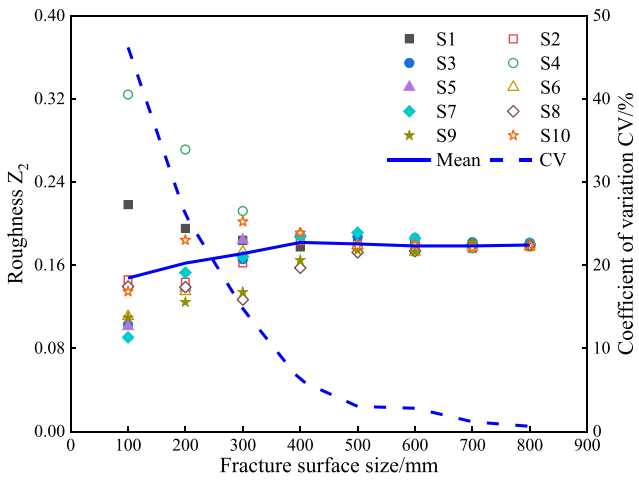
$$Q = A \frac{k}{\mu} \frac{\Delta P}{L} \tag{8}$$



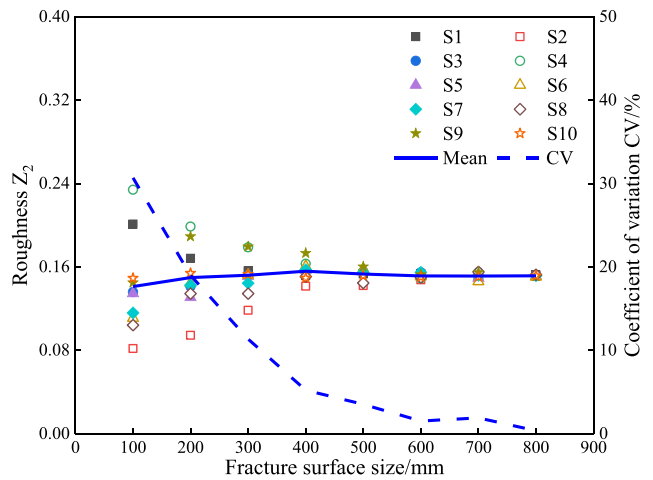
(a) A2-x



(b) A2-y



(c) C3-x



(d) C3-y

Fig. 13 Relation between roughness and fracture surface sizes on fracture surfaces A2 and C3 along the x-axis and y-axis

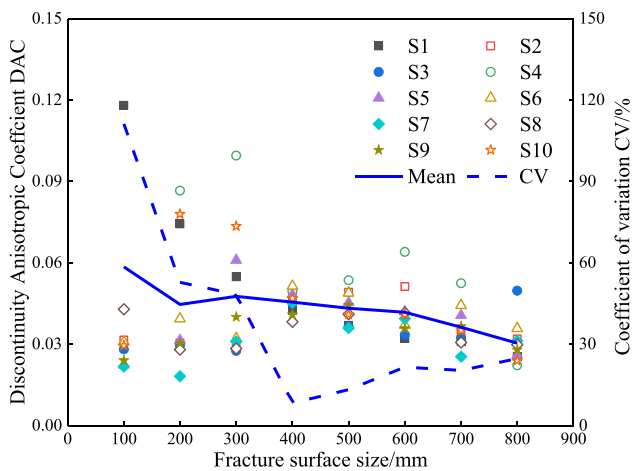


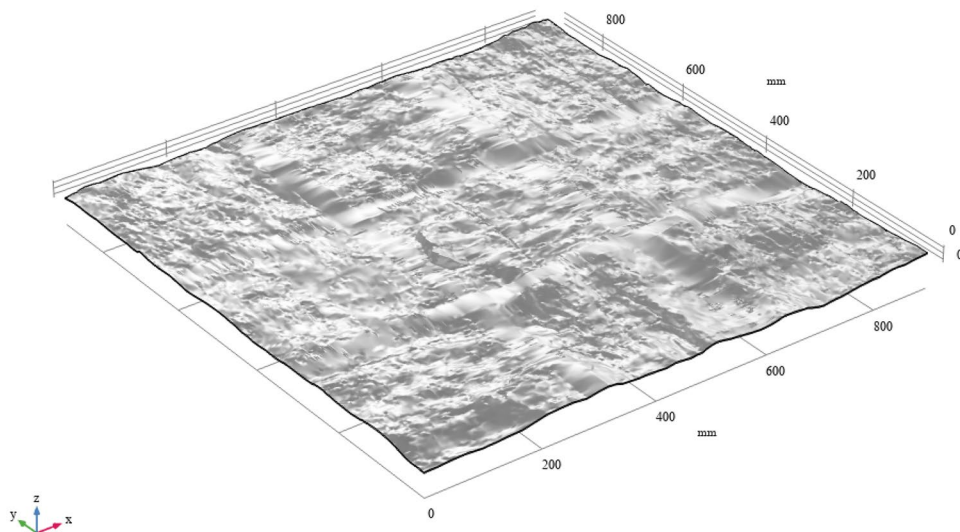
Fig. 14 Discontinuity anisotropic coefficient with different sizes on fracture surface C3

where, A is the cross-sectional area, L is the fracture size. It is necessary to calculate the permeability of fractures with different sizes to investigate the size effect on fracture permeability. The pressure gradient should be consistent when calculating the permeability of fractures with different sizes.

Fracture models and boundary conditions

The fracture model was obtained by translating the scanned fracture surface to a certain distance using the FEM software COMSOL Multiphysics, as shown in Fig. 15. The rough fracture model in Fig. 15 was obtained by translating fracture surface C3 1 mm along the z-axis, and its size was $900 \times 900 \times 1$ mm. To be noted, the fracture size is represented by the side length of the fracture surface.

Fig. 15 Rough fracture model obtained by translating fracture surface C3 1 mm along the z-axis



The size of the “base” fracture model was 900 mm. The sampling fracture models with different sizes were obtained in the same way as the sampling fracture surface, which is shown in Fig. 9. The permeability in two directions needs to be obtained and two different boundary conditions were considered: unidirectional flow along the x-axis and y-axis. For all sampling fracture models with different sizes, a constant pressure gradient was maintained between the inlet and outlet boundaries, and other boundaries were fixed with impervious conditions (Huang et al. 2018; Wang et al. 2018b).

Size effect on the permeability

The flow rate at the outlet can be easily obtained by numerical simulation, and the permeability can be calculated according to Eq. (8). The results are shown in Fig. 16.

The permeability along the x-axis and y-axis with different model sizes is shown in Fig. 16. The permeability of the fracture varies significantly at small fracture sizes. As the fracture size increases, the permeability tends toward a relatively stable state. The results are the same as those of the fracture surface roughness. As the result of the roughness size effect, the

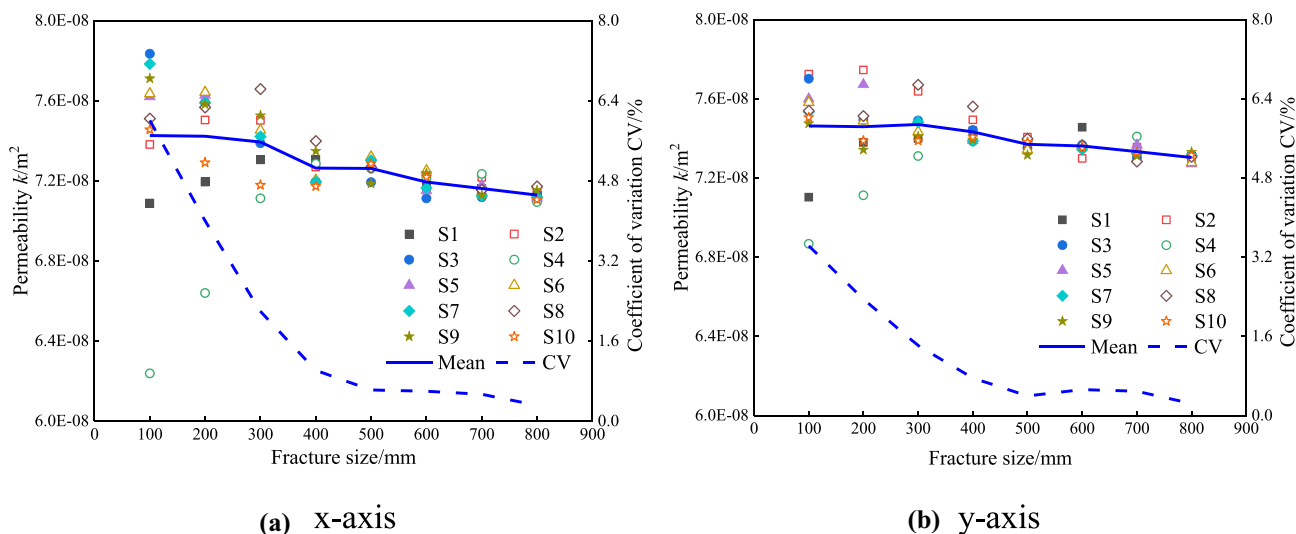


Fig. 16 Relation between permeability along the (a) x-axis and (b) y-axis and fracture model size

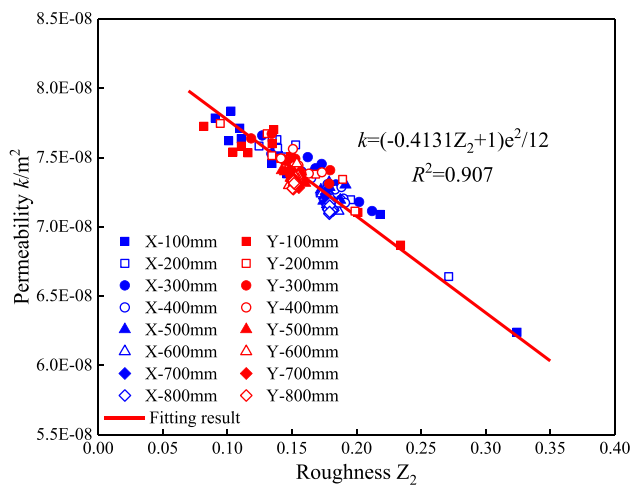


Fig. 17 Relation between the permeability of the sampling fracture models and roughness of the corresponding sampling fracture surface

variation coefficient of 15% and difference between the sampling size and the next sampling size of 5% are used as the criterion for permeability to enter the stable state (Baghbanan and Jing 2007; Koyama and Jing 2007; Liang et al. 2019). The variation coefficient of permeability with different sizes is less than 15% and even less than 5%. The RES size for permeability is less than 100 mm considering the criterion of the variation coefficient. According to Young et al. (2020), 10–20% CV criterion has generally been used to determine the RES sizes for the fracture rock parameter, but a CV of 2.5% or lower may provide the best estimate of the RES size for fracture permeability. The criterion of the variation coefficient for fracture permeability is 2.5% in this study. The RES sizes for permeability along the x-axis and y-axis are 300 and 300 mm, respectively. The RES sizes for permeability using the 2.5% CV criterion are equal to those for roughness using the 15% CV criterion. The equivalent permeabilities of the fracture along the x-axis and y-axis are 7.23×10^{-8} and 7.39×10^{-8} m², respectively. The relation between the permeability of the sampling fracture models and the roughness of the corresponding sampling fracture surface is shown in Fig. 17.

The fracture permeability decreases linearly with the fracture surface roughness according to Fig. 17. There is little difference in the relation between fracture permeability and fracture surface roughness with different sizes. It can be considered that the reason for the permeability difference of different sizes is the roughness difference of the fracture surface. A linear function was used to fit the relation between fracture permeability and fracture surface roughness, as shown in Eq. (9). When the fracture surface roughness is equal to zero, i.e. the fracture consists of a pair

of smooth parallel surfaces with an aperture of 1 mm, the fracture permeability is 8.33×10^{-8} m², which is equal to $e^2/12$ ($e = 1$ mm) (Jing and Stephansson 2007).

$$k = \frac{(a \cdot Z_2 + 1)e^2}{12} \quad (9)$$

where a is the linear fitting parameter, which is equal to -0.4131 in this study.

Discussion

The lithology of the rock wall of the scanned fracture surface is quartz sandstone, and the fracture surface is flat. Due to weathering, the mineral particles and local undulation on the fracture surface are larger than those on the fresh fracture surface. The rock weathering in area A is more serious than that in area C, and the RES size of fracture surface A2 is larger than that of fracture surface C3. This indicates that weathering affects the RES size for fracture surface morphology. The RES size for fracture surfaces with different rock lithologies may be different. The RES size for the fractal parameters of the fracture surface is approximately 500 mm (Fardin et al. 2001). The lithology of the rock wall is granite. The mineral particles are small, and the fracture surface is more uneven than the scanned fracture surface in the study. This may be one of the reasons why the RES for fractal parameters is larger than that for fracture surface morphology in the study. In addition, the RES for fracture surface morphology does not exist on all fracture surfaces. For example, due to the strong roughness anisotropy of the fracture surface with plumose structure, the RES size for fracture surface morphology will be large or may not exist.

This study focuses on the size effect of fracture surface morphology and hydraulic behavior. The influence of morphology on the effect of fracture permeability was also investigated. The strength of fractures also exhibits a strong correlation with the size, and the fracture surface morphology influences the size effect of fracture strength (Özvan et al. 2014; Wei et al. 2022). Lin et al. (2019) and Ueng et al. (2010) found that there is a size effect on the shear strength of the fracture surface and that the size effect is related to the morphology of the fracture surface. Some asperities were destroyed during the shear test, and the fracture surface after shear was smoother than the initial fracture surface. It is speculated that the RES for the shear strength of the fracture surface may be smaller than the RES for fracture surface morphology.

Conclusion

Based on the asperity height data of a fracture surface obtained by 3D laser scanning in the field, the size effect on the morphology of the fracture surfaces was analyzed, including the size effect on the asperity height distribution, roughness and anisotropy of the fracture surfaces. The asperity heights of most fracture surfaces with different sizes followed a normal distribution and the asperity height distribution tended to be consistent with the increase in fracture size. The roughness of the fracture surfaces varied significantly at small fracture surface sizes. As the fracture surface size increase, fracture surface roughness tended toward a relatively stable state. The roughness variation coefficient of 15% was taken as the criterion for the roughness to enter a stable state, and the RES size for the fracture surface roughness was 300–400 mm.

A rough single fracture model was established based on the scanned fracture surface data, and the relation between fracture permeability and fracture size was analyzed. The permeability of the fracture varied significantly at the fracture sizes. As the fracture size increases, the permeability tended toward a relatively stable state. These results were the same as those of the fracture surface roughness. The permeability variation coefficient of 2.5% provided the best estimate of the RES size for fracture permeability, and the RES size for permeability was determined to be approximately 300 mm. The relation between permeability and roughness was analyzed, and the permeability difference at different sizes was caused by the different roughnesses of the fracture surfaces.

Comparing the size effect on fracture surface roughness with that on permeability, the roughness and permeability vary with the sizes of fracture and RES sizes for roughness and permeability both exist. If the unified CV criterion is used to estimate the RES sizes, the RES size for permeability is much smaller than that for roughness. Although the roughness and permeability vary with size, there are obvious differences in the range of variation. The variation range of roughness with size is $\pm 35\%$, and that of permeability is $\pm 2\%$. The variation range of permeability is much smaller than that of roughness, so the criterion for determining RES sizes for permeability needs to be stricter than that for roughness. The reason why the permeability variation range is much smaller than that of roughness may be related to the accuracy of the grid in the numerical simulation.

Funding This study was financially supported by the National Natural Science Foundation of China with No. 42177157 and 51779045, the Fundamental Research Funds for the Central Universities with Nos. N2001025, N2001026 and N2101005, Applied Basic Research Program of Liaoning Province with No. 2022020363-JH2/1013, Innovative

Talents Support Program of Sciences & Technologies of Shenyang Young and Middle-aged Scientists with No. RC210405, and Shenyang Science and Technology Program with No. 22-322-3-17.

Declarations

Conflict of interest The authors declare no competing interests.

References

- Alameda-Hernández P, Jiménez-Perálvarez J, Palenzuela JA, El Hamdouni R, Irigaray C, Cabrerizo MA, Chacón J (2014) Improvement of the JRC calculation using different parameters obtained through a new survey method applied to rock discontinuities. *Rock Mech Rock Eng* 47:2047–2060. <https://doi.org/10.1007/s00603-013-0532-2>
- Babanouri N, Karimi Nasab S, Sarafrazi S (2013) A hybrid particle swarm optimization and multi-layer perceptron algorithm for bivariate fractal analysis of rock fractures roughness. *Int J Rock Mech Min Sci* 60:66–74. <https://doi.org/10.1016/j.ijrmms.2012.12.028>
- Baghbanan A, Jing L (2007) Hydraulic properties of fractured rock masses with correlated fracture length and aperture. *Int J Rock Mech Min Sci* 44:704–719. <https://doi.org/10.1016/j.ijrmms.2006.11.001>
- Barton N (1973) Review of a new shear-strength criterion for rock joints. *Eng Geol* 7:287–332. [https://doi.org/10.1016/0013-7952\(73\)90013-6](https://doi.org/10.1016/0013-7952(73)90013-6)
- Belem T, Homand-Etienne F, Souley M (2000) Quantitative parameters for rock joint surface roughness. *Rock Mech Rock Eng* 33:217–242. <https://doi.org/10.1007/s006030070001>
- Berkowitz B (2002) Characterizing flow and transport in fractured geological media: a review. *Adv Water Resour* 25:861–884. [https://doi.org/10.1016/S0309-1708\(02\)00042-8](https://doi.org/10.1016/S0309-1708(02)00042-8)
- Brown SR (1987) Fluid flow through rock joints: the effect of surface roughness. *J Geophys Res Solid Earth* 92:1337–1347. <https://doi.org/10.1029/JB092iB02p01337>
- Brown SR, Scholz CH (1985) Broad bandwidth study of the topography of natural rock surfaces. *J Geophys Res Solid Earth* 90:12575–12582. <https://doi.org/10.1029/JB090iB14p12575>
- Chen S, Zhu W, Liu S, Zhang F, Guo L (2015a) Anisotropy and Size Effects of Surface Roughness of Rock Joints. *Chin J Rock Mech Eng* 34:57–66
- Chen SJ, Zhu WC, Yu QL, Liu XG (2016) Characterization of anisotropy of joint surface roughness and aperture by variogram approach based on digital image processing technique. *Rock Mech Rock Eng* 49:855–876. <https://doi.org/10.1007/s00603-015-0795-x>
- Chen T, Feng X-T, Cui G, Tan Y, Pan Z (2019) Experimental study of permeability change of organic-rich gas shales under high effective stress. *J Nat Gas Sci Eng* 64:1–14. <https://doi.org/10.1016/j.jngse.2019.01.014>
- Chen Y-F, Zhou J-Q, Hu S-H, Hu R, Zhou C-B (2015b) Evaluation of Forchheimer equation coefficients for non-Darcy flow in deformable rough-walled fractures. *J Hydrol* 529:993–1006. <https://doi.org/10.1016/j.jhydrol.2015.09.021>
- Dou Z, Sleep B, Zhan H, Zhou Z, Wang J (2019) Multiscale roughness influence on conservative solute transport in self-affine fractures. *Int J Heat Mass Transf* 133:606–618. <https://doi.org/10.1016/j.ijheatmasstransfer.2018.12.141>
- Esmaili K, Hadjigeorgiou J, Grenon M (2010) Estimating geometrical and mechanical REV based on synthetic rock mass models at

- Brunswick Mine. *Int J Rock Mech Min Sci* 47:915–926. <https://doi.org/10.1016/j.ijrmmms.2010.05.010>
- Fakhimi A, Gharahbagh EA (2011) Discrete element analysis of the effect of pore size and pore distribution on the mechanical behavior of rock. *Int J Rock Mech Min Sci* 48:77–85. <https://doi.org/10.1016/j.ijrmmms.2010.08.007>
- Fardin N, Stephansson O, Jing LR (2001) The scale dependence of rock joint surface roughness. *Int J Rock Mech Min Sci* 38:659–669. [https://doi.org/10.1016/S1365-1609\(01\)00028-4](https://doi.org/10.1016/S1365-1609(01)00028-4)
- Feng P, Zhao J, Dai F, Wei M, Liu B (2022) Mechanical behaviors of conjugate-flawed rocks subjected to coupled static–dynamic compression. *Acta Geotech* 17:1765–1784. <https://doi.org/10.1007/s11440-021-01322-6>
- Giwelli AA, Sakaguchi K, Matsuki K (2009) Experimental study of the effect of fracture size on closure behavior of a tensile fracture under normal stress. *Int J Rock Mech Min Sci* 46:462–470. <https://doi.org/10.1016/j.ijrmmms.2008.11.008>
- Huang N, Jiang Y, Liu R, Li B (2017) Estimation of permeability of 3-D discrete fracture networks: an alternative possibility based on trace map analysis. *Eng Geol* 226:12–19. <https://doi.org/10.1016/j.enggeo.2017.05.005>
- Huang NA, Jiang Y, Liu R, Xia Y (2018) Size effect on the permeability and shear induced flow anisotropy of fractal rock fractures. *Fractals* 26:1840001. <https://doi.org/10.1142/S0218348X18400017>
- Jing L, Stephansson O (2007) Fundamentals of discrete element method for engineering: Theory and Applications. Elsevier Science
- Koyama T, Jing L (2007) Effects of model scale and particle size on micro-mechanical properties and failure processes of rocks—a particle mechanics approach. *Eng Anal Bound Elem* 31:458–472. <https://doi.org/10.1016/j.enganabound.2006.11.009>
- Kulatilake PHSW, Balasingam P, Park J, Morgan R (2006) Natural rock joint roughness quantification through fractal techniques. *Geotech Geol Eng* 24:1181–1202. <https://doi.org/10.1007/s10706-005-1219-6>
- Lei Q, Latham J-P, Tsang C-F, Xiang J, Lang P (2015) A new approach to upscaling fracture network models while preserving geostatistical and geomechanical characteristics. *J Geophys Res Solid Earth* 120:4784–4807. <https://doi.org/10.1002/2014JB011736>
- Li B, Mo Y, Zou L, Liu R, Cvetkovic V (2020a) Influence of surface roughness on fluid flow and solute transport through 3D crossed rock fractures. *J Hydrol* 582:124284. <https://doi.org/10.1016/j.jhydrol.2019.124284>
- Li Y, Sun S, Yang H (2020b) Scale dependence of waviness and unevenness of natural rock joints through fractal analysis. *Geofluids* 2020:8818815. <https://doi.org/10.1155/2020/8818815>
- Li Y, Zhang Y (2015) Quantitative estimation of joint roughness coefficient using statistical parameters. *Int J Rock Mech Min Sci* 77:27–35. <https://doi.org/10.1016/j.ijrmmms.2015.03.016>
- Liang Z, Wu N, Li Y, Li H, Li W (2019) Numerical study on anisotropy of the representative elementary volume of strength and deformability of jointed rock masses. *Rock Mech Rock Eng* 52:4387–4402. <https://doi.org/10.1007/s00603-019-01859-9>
- Lin H, Xie S, Yong R, Chen Y, Du S (2019) An empirical statistical constitutive relationship for rock joint shearing considering scale effect. *Comptes Rendus Mécanique* 347:561–575. <https://doi.org/10.1016/j.crme.2019.08.001>
- Liu J, Wang Z, Qiao L, Li W, Yang J (2021) Transition from linear to nonlinear flow in single rough fractures: effect of fracture roughness. *Hydrogeol J* 29:1343–1353. <https://doi.org/10.1007/s10040-020-02297-6>
- Liu R, Huang N, Jiang Y, Jing H, Yu L (2020) A numerical study of shear-induced evolutions of geometric and hydraulic properties of self-affine rough-walled rock fractures. *Int J Rock Mech Mining Sci* 127:104211. <https://doi.org/10.1016/j.ijrmmms.2020.104211>
- Liu R, Li B, Jiang Y, Huang N (2016) Review: Mathematical expressions for estimating equivalent permeability of rock fracture networks. *Hydrogeol J* 24:1623–1649. <https://doi.org/10.1007/s10040-016-1441-8>
- Liu R, Yu L, Jiang Y, Wang Y, Li B (2017) Recent developments on relationships between the equivalent permeability and fractal dimension of two-dimensional rock fracture networks. *J Nat Gas Sci Eng* 45:771–785. <https://doi.org/10.1016/j.jngse.2017.06.013>
- Luo S, Zhao Z, Peng H, Pu H (2016) The role of fracture surface roughness in macroscopic fluid flow and heat transfer in fractured rocks. *Int J Rock Mech Min Sci* 87:29–38. <https://doi.org/10.1016/j.ijrmmms.2016.05.006>
- Nigon B, Englert A, Pascal C, Saintot A (2017) Multiscale characterization of joint surface roughness. *J Geophys Res Solid Earth* 122:9714–9728. <https://doi.org/10.1002/2017JB014322>
- Odling NE (1994) Natural fracture profiles, fractal dimension and joint roughness coefficients. *Rock Mech Rock Eng* 27:135–153. <https://doi.org/10.1007/BF01020307>
- Özvan A, Dinçer İ, Acar A, Özvan B (2014) The effects of discontinuity surface roughness on the shear strength of weathered granite joints. *Bull Eng Geol Env* 73:801–813. <https://doi.org/10.1007/s10064-013-0560-x>
- Pandey SN, Vishal V, Chaudhuri A (2018) Geothermal reservoir modeling in a coupled thermo-hydro-mechanical-chemical approach: a review. *Earth-Sci Rev* 185:1157–1169. <https://doi.org/10.1016/j.earscirev.2018.09.004>
- Qian J, Zhan H, Luo S, Zhao W (2007) Experimental evidence of scale-dependent hydraulic conductivity for fully developed turbulent flow in a single fracture. *J Hydrol* 339:206–215. <https://doi.org/10.1016/j.jhydrol.2007.03.015>
- Raven KG, Gale JE (1985) Water Flow in a Natural Rock Fracture as a Function of Stress and Sample Size. *Int J Rock Mech Mining Sci Geomecha Abstracts* 22:251–261. [https://doi.org/10.1016/0148-9062\(85\)92952-3](https://doi.org/10.1016/0148-9062(85)92952-3)
- Rong G, Peng J, Wang X, Liu G, Hou D (2013) Permeability tensor and representative elementary volume of fractured rock masses. *Hydrogeol J* 21:1655–1671. <https://doi.org/10.1007/s10040-013-1040-x>
- Singh H, Cai J (2018) Screening improved recovery methods in tight-oil formations by injecting and producing through fractures. *Int J Heat Mass Transf* 116:977–993. <https://doi.org/10.1016/j.ijheatmasstransfer.2017.09.071>
- Song L, Jiang Q, Li L-f, Liu C, Liu X-p, Xiong J (2020) An Enhanced Index for Evaluating Natural Joint Roughness Considering Multiple Morphological Factors Affecting the Shear Behavior. *Bull Eng Geol Environ* 79:2037–2057. <https://doi.org/10.1007/s10064-019-01700-1>
- Song L, Jiang Q, Li Y, Yang C, Zhong S, ZHANG M (2017) Study on the Stability of Statistical Parameters of the Rock Nature Discontinuities Morphology and Anisotropic Based on Different Interval Point-Cloud Data. *Rock Soil Mech* 38:1–13
- Sutopo, Arihara N, Sato K, Abbaszadeh M (2002) Representative elementary volume of naturally fractured reservoirs evaluated by flow simulation. *J Jpn Pet Inst* 45:156–168. <https://doi.org/10.1627/jpi.45.156>
- Tatone BSA, Grasselli G (2010) A new 2D discontinuity roughness parameter and its correlation with JRC. *Int J Rock Mech Mining Sci* 47:1391–1400. <https://doi.org/10.1016/j.ijrmmms.2010.06.006>
- Thomas TR (1981) Characterization of Surface Roughness Precision Engineering 3:97–104. [https://doi.org/10.1016/0141-6359\(81\)90043-X](https://doi.org/10.1016/0141-6359(81)90043-X)
- Tsang YW, Witherspoon PA (1983) The dependence of fracture mechanical and fluid flow properties on fracture roughness and sample size. *J Geophys Res: Solid Earth* 88:2359–2366. <https://doi.org/10.1029/JB088iB03p02359>
- Ueng T-S, Jou Y-J, Peng IH (2010) Scale effect on shear strength of computer-aided-manufactured joints. *J GeoEng* 5:29–37. [https://doi.org/10.6310/jog.2010.5\(2\).1](https://doi.org/10.6310/jog.2010.5(2).1)

- Vogler D, Settgast RR, Annavarapu C, Madonna C, Bayer P, Amann F (2018) Experiments and simulations of fully hydro-mechanically coupled response of rough fractures exposed to high-pressure fluid injection. *J Geophys Res: Solid Earth* 123:1186–1200. <https://doi.org/10.1002/2017JB015057>
- Wang C, Jiang Y, Liu R, Wang C, Zhang Z, Sugimoto S (2020) Experimental study of the nonlinear flow characteristics of fluid in 3D rough-walled fractures during shear process. *Rock Mech Rock Eng* 53:2581–2604. <https://doi.org/10.1007/s00603-020-02068-5>
- Wang M, Chen Y-F, Ma G-W, Zhou J-Q, Zhou C-B (2016) Influence of surface roughness on nonlinear flow behaviors in 3D self-affine rough fractures: lattice Boltzmann simulations. *Adv Water Resour* 96:373–388. <https://doi.org/10.1016/j.advwatres.2016.08.006>
- Wang Z, Li W, Bi L, Qiao L, Liu R, Liu J (2018a) Estimation of the REV size and equivalent permeability coefficient of fractured rock masses with an emphasis on comparing the radial and unidirectional flow configurations. *Rock Mech Rock Eng* 51:1457–1471. <https://doi.org/10.1007/s00603-018-1422-4>
- Wang Z, Li W, Qiao L, Liu J, Yang J (2018b) Hydraulic properties of fractured rock mass with correlated fracture length and aperture in both radial and unidirectional flow configurations. *Comput Geotech* 104:167–184. <https://doi.org/10.1016/j.compgeo.2018.08.017>
- Wei M, Dai F, Liu Y, Jiang R (2022) A fracture model for assessing tensile mode crack growth resistance of rocks. *J Rock Mech Geotech Eng*. <https://doi.org/10.1016/j.jrmge.2022.03.001>
- Wei M, Dai F, Liu Y, Li A, Yan Z (2021) Influences of loading method and notch type on rock fracture toughness measurements: from the perspectives of t-stress and fracture process zone. *Rock Mech Rock Eng* 54:4965–4986. <https://doi.org/10.1007/s00603-021-02541-9>
- Witherspoon PA, Wang JSY, Iwai K, Gale JE (1980) Validity of Cubic Law for fluid flow in a deformable rock fracture. *Water Resour Res* 16:1016–1024. <https://doi.org/10.1029/WR016i006p01016>
- Wu C, Chu J, Wu S, Hong Y (2019) 3D characterization of microbially induced carbonate precipitation in rock fracture and the resulted permeability reduction. *Eng Geol* 249:23–30. <https://doi.org/10.1016/j.enggeo.2018.12.017>
- Yan F, Ban L, Qi C, Shan R, Yuan H (2020) Research on the anisotropy, size effect, and sampling interval effect of joint surface roughness. *Arab J Geosci* 13:399. <https://doi.org/10.1007/s12517-020-05330-w>
- Yang ZY, Di CC, Yen KC (2001) The effect of asperity order on the roughness of rock joints. *Int J Rock Mech Min Sci* 38:745–752. [https://doi.org/10.1016/S1365-1609\(01\)00032-6](https://doi.org/10.1016/S1365-1609(01)00032-6)
- Young NL, Simpkins WW, Reber JE, Helmke MF (2020) Estimation of the representative elementary volume of a fractured till: a field and groundwater modeling approach. *Hydrogeol J* 28:781–793. <https://doi.org/10.1007/s10040-019-02076-y>
- Zhang G, Karakus M, Tang H, Ge Y, Zhang L (2014) A new method estimating the 2D Joint Roughness Coefficient for discontinuity surfaces in rock masses. *Int J Rock Mech Mining Sci* 72:191–198. <https://doi.org/10.1016/j.ijrmms.2014.09.009>
- Zhao L et al (2020) A practical photogrammetric workflow in the field for the construction of a 3D rock joint surface database. *Eng Geol* 279:105878. <https://doi.org/10.1016/j.enggeo.2020.105878>
- Zhao L, Zhang S, Huang D, Zuo S, Li D (2018) Quantitative characterization of joint roughness based on semivariogram parameters. *Int J Rock Mech Min Sci* 109:1–8. <https://doi.org/10.1016/j.ijrmms.2018.06.008>
- Zou L, Håkansson U, Cvetkovic V (2020) Radial propagation of yield-power-law grouts into water-saturated homogeneous fractures. *Int J Rock Mech Mining Sci* 130:104308. <https://doi.org/10.1016/j.ijrmms.2020.104308>
- Zou L, Jing L, Cvetkovic V (2015) Roughness decomposition and nonlinear fluid flow in a single rock fracture. *Int J Rock Mech Min Sci* 75:102–118. <https://doi.org/10.1016/j.ijrmms.2015.01.016>
- Springer Nature or its licensor (e.g. a society or other partner) holds exclusive rights to this article under a publishing agreement with the author(s) or other rightsholder(s); author self-archiving of the accepted manuscript version of this article is solely governed by the terms of such publishing agreement and applicable law.